The bifurcation of circular jets in crossflow

Pablo Huq and M. R. Dhanak

Citation: Phys. Fluids **8**, 754 (1996); doi: 10.1063/1.868859
View online: http://dx.doi.org/10.1063/1.868859
View Table of Contents: http://pof.aip.org/resource/1/PHFLE6/v8/i3
Published by the American Institute of Physics.

The bifurcation of circular jets in crossflow

Pablo Huq
College of Marine Studies, University of Delaware, Newark, Delaware 19716

M. R. Dhanak
Department of Ocean Engineering, Florida Atlantic University, Boca Raton, Florida 33431

(Received 3 May 1994; accepted 28 November 1995)

An experimental study of an incompressible circular jet in a crossflow and theoretical analysis based on inviscid flow models are described. The jet exits from a rigidly mounted pipe projecting distant from the floor of a tunnel carrying a steady stream of water; density of the jet and the stream are the same. The results of scalar and velocity measurements and visualizations showed that the jet bifurcated into two separated, counterrotating arms for values of $\epsilon = U_\infty / U_{\mathrm{JET}}$, the ratio of the mean crossflow velocity U_∞ to the mean jet discharge velocity U_{JET}, less than or equal to 0.25. The angle of separation between the two arms of the bifurcated jet was found to vary inversely with ϵ. For higher values of ϵ the jet does not bifurcate but is dominated by a different mode of instability. The structure of the flow field, which is different for bifurcated and nonbifurcated jets, comprised a variety of vortical structures which survived for very long distances x beyond $x/2a > 400$, where a is the radius of the jet exit and x is distance downstream from the jet axis. The location of the point of bifurcation is predicted from consideration of potential flow models and the characteristics of bifurcating elliptical jets. The location of the point of bifurcation is more distant from the jet exit for smaller values of ϵ, and experimental results were in good agreement with the theoretical predictions. The initial jet trajectory is shown to be associated with the presence in the wake of vorticity shed from the pipe. The near-field geometry and centerline trajectory of the jet are also found to be in accord with predictions in that it is observed that $z \sim x^{1/2}$ and $z \sim \epsilon^{-1}$. Dilutions of bifurcated jets are found to be greater than for nonbifurcated jets. © *1996 American Institute of Physics.* [S1070-6631(96)01403-0]

I. INTRODUCTION

Interest in the nature of the flow of an incompressible transverse jet in a cross-flow persists due to an incomplete understanding of the dynamics of jet–cross-flow interaction. Such interactions are pertinent to jets of VTOL aircraft, to discharges from chimney stacks to the atmosphere, and to disposal via diffusers of sewage into rivers and estuaries. The frequent occurrence of jet flows into a cross-flow has led to numerous previous studies. Experiments have been conducted by Keffer and Baines,[1] McMahon *et al.*,[2] Kamotani and Greber,[3] Fearn and Weston,[4] Chassaing *et al.*,[5] Moussa *et al.*,[6] Crabb *et al.*,[7] Andreopoulous and Rodi,[8] and Fric and Roshko.[9] A consensus view is that a pair of counter-rotating vortices eventually dominates the flow field. In the above experimental studies, the experimental configuration typically comprised a circular jet whose exit was either flush with the floor of the (wind) tunnel (e.g., Ref. 9 or from a pipe projecting above the floor of the tunnel, e.g., Ref. 6). Fric and Roshko[9] found that no vortex shedding occurs from the jet surface. However, there remains questions about the flow field, in particular of the interpretation that the wake of the jet features vortical structures which arise from the bottom boundary layer in the former case, and from shedding off the rigid pipe in the latter case.[10]

In the present experiment the jet exit was located some ten jet diameters (i.e., $20a$, where a is the radius of the jet exit) from the floor of the tunnel. This resulted in the jet exit being located outside the bottom boundary layer in a region of uniform velocity, the typical bottom boundary layer thickness being $10a$ (see Fig. 1). The present study, in accord with observations from chimney stacks, shows that under such conditions the jet can bifurcate, i.e., split into two distinct arms. The mechanics of the bifurcation of jets are not well understood. It has been suggested that bifurcation arises from buoyancy-induced circulation[11] or can be induced by acoustic forcing or vibration.[12] We show, however, that buoyancy is not necessary for the occurrence of bifurcation of a transverse jet in cross-flow and establish a criterion for this occurrence; the pipe in our experiments was rigidly mounted, and there was no acoustic forcing. We show that bifurcation of the jet occurs when the value of $\epsilon \leqslant 0.25$ where $\epsilon = U_\infty / U_{\mathrm{JET}}$. We analyzed the dynamics of the near field of the jet utilizing existing potential flow models, and conducted experiments to verify the analysis.

II. APPROXIMATE ANALYSIS FOR NEAR JET REGION

Potential flow models of the jet in the vicinity of the orifice have been developed by Chang-Lu,[13] Needham *et al.*,[14] and Coelho and Hunt.[15] Chang-Lu's model is based on two-dimensional (2-D) considerations involving the evolution in time of the jet boundary which is represented by a 2-D vortex sheet. The evolution of a circular vortex sheet is obtained as an asymptotic series in time, t, for small times and is related to the spatial development of the jet with the distance z from the orifice through the transformation $z = U_{\mathrm{jet}} t/2$. If $\epsilon = U_\infty / U_{\mathrm{jet}} \ll 1$ and $\xi = \epsilon z / a$ denotes a scaled

 1070-6631/96/8(3)/754/10/$10.00

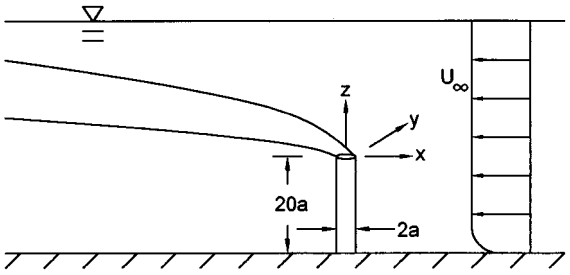

FIG. 1. Flow configuration and coordinate system.

nondimensional distance from the orifice (Figs. 1 and 2), the jet boundary at a fixed value of ξ, according to Chang-Lu's model is given by $r=r_b(\theta,\xi)$ where

$$r_b(\theta,\xi)/a=1-2\xi^2\cos 2\theta-\frac{4}{3}\xi^3(3\cos 3\theta-\cos\theta)+O(\xi^4) \tag{1}$$

in terms of polar coordinates (r,θ). It may be noted that the shape is not symmetric about the y axis (see Fig. 2). Furthermore, the model predicts only a small shift [at $O(\xi^3)$] in the position of the jet center. If three-dimensionality is properly accounted for in the potential flow model, then it is found that the cross-sectional shape of the jet remains symmetric about the y axis and no shift in the center occurs, at least to $O(\xi^4)$. According to Needham *et al.*,[14] the shape of the jet is given by

$$r_b(\theta,\xi)/a=1-\xi^2\cos 2\theta+O(\xi^4). \tag{2}$$

This model assumes that the difference between the ambient pressures outside and inside the pipe, away from the orifice is $O(\rho_{\text{jet}}U_{\text{jet}}^2\epsilon^2)$.

The plan view of the jet as predicted by models (1) (dashed curve) and (2) (solid line) are shown in Fig. 3. The corresponding side views, in x-z plane, and front views in y-z plane, are shown in Figs. 4(a)–4(d) respectively. The 3-D model fails to predict the observed asymmetry of the jet cross-section about the y axis as well as the downstream development of the jet, both of which, as we discuss below, are related to the presence, in the near wake, of vortices associated with separation off the cylindrical pipe. However, the model does predict the initial deformation of the jet by the cross-flow whereby its cross-section becomes elliptical. The aspect ratio of the ellipse increases with distance from the jet exit. We believe that this deformation has an important bearing on the development of the instability of the jet and the wake development, in view of the known instability of a jet of elliptical cross-section of sufficiently large aspect ratio which in the absence of any cross-flow, leads to bifurcation of the jet.

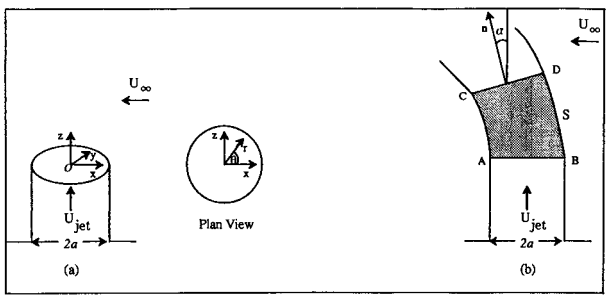

FIG. 2. Definition sketch of variables used in analysis of near-field of jet. The shaded region is the control volume V enclosed by jet surfaces.

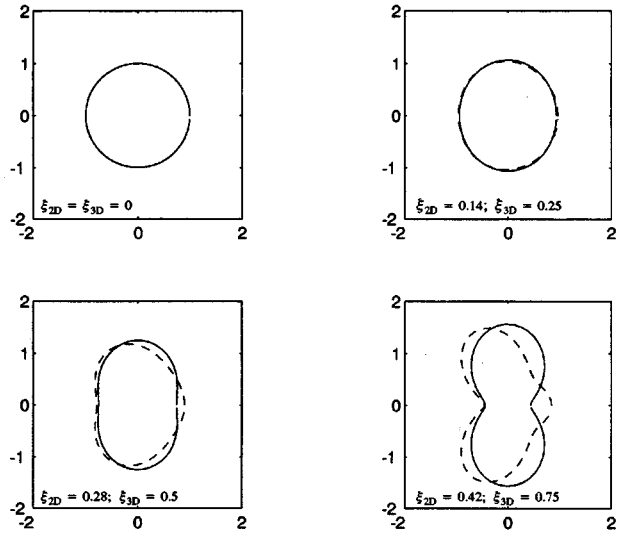

FIG. 3. Plan view of the jet according to the 2-D model [(----); Eq. (1)] at $\xi=\xi_{2D}$ and 3-D model [——; Eq. (2)] at $\xi=\xi_{3D}$ for various values of nondimensional height ξ.

In their detailed measurements of the turbulent velocity field of elliptic jets, in the absence of a cross-flow, Hussain and Husain[16] showed that the azimuthal curvature variation of the elliptic cross section, of the jet induced velocities resulting in complex three-dimensional deformation, and ultimately bifurcation for cross sections of sufficiently large aspect ratio. Thus if we assume that bifurcation is primarily

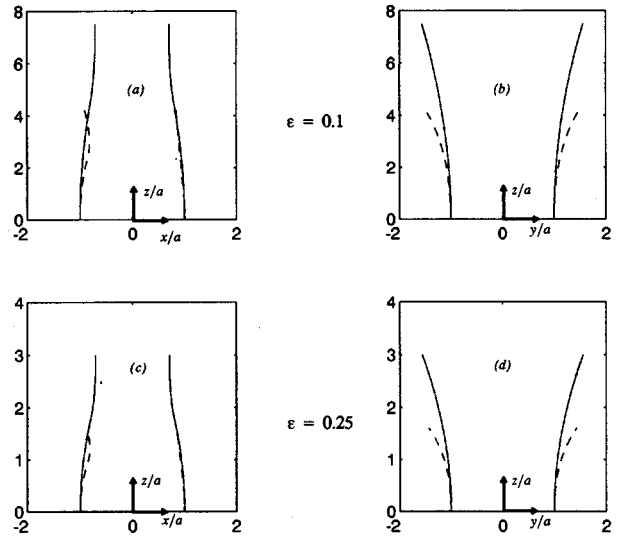

FIG. 4. Side [(a) and (c)] and windward [(b) and (d)] views of the jet according to the 2-D model [----; Eq. (1)] for the range $0\leqslant z\epsilon/a\leqslant 0.42$ and 3-D model [——; Eq. (2)] for the range $0\leqslant z\epsilon/a\leqslant 0.75$ for two values of ϵ. The predicted plan view corresponding to the final value of z/a in each case is shown in Fig. 3(d).

associated with the cross-sectional shape of the jet even though the initial instability may be associated with the vortex wake downstream of the jet, and that the criteria for bifurcation of elliptical jets approximately holds for circular jets in cross-flow, we can predict the location of bifurcation in the latter case.

As the distance from the orifice increases, the ellipticity or aspect ratio $\alpha = r_b(\pi/2,\xi)/r_b(0,\xi)$ gets larger. For an elliptical jet of aspect ratio α, Hussain and Husain[16] suggest that the jet bifurcates if $\alpha > 3.5$. Since the cross-flow makes the circular jet elliptical, if we assume that this criteria approximately still applies, then we can estimate that the jet will bifurcate at $\xi = > 0.75$ according to the 3-D model and at $\xi > 0.437$, according to the 2-D model. The final subplot in Fig. 3 depicts the stage when this critical aspect ratio is approximately attained for each model; the other subplots depict the shapes at equal intervals in ξ. (The position at which bifurcation actually occurred in the experiments was determined and the results are compared with these predictions in Fig. 9.) The agreement with the 3-D model is fairly good, giving support to the criteria suggested here.

The potential flow models fail to predict the observed initial displacement of the jet. Coelho and Hunt[15] suggest a turbulence entrainment model involving mass transfer to account for this discrepancy. However, we show that the presence of the wake vorticity in the near jet region contributes to the initial jet displacement; eventually, as mass and momentum transfer occur, the displacement mechanism of Coelho and Hunt[15] will become important. We assume, however, that close to the orifice, for $\epsilon \ll 1$, mass transfer is not significant and that the jet displacement is predominantly governed by form or pressure drag due to the presence of vortices in the wake of the cylindrical pipe.

If $d(z)$ is the transverse (in y-z plane) breadth of the jet, then the pressure drag experienced by length dz of the jet due to the presence of vortices in the wake can be written

$$D = \frac{1}{2}\,\rho U_\infty^2 d(z) c_D\,, \tag{3}$$

where c_D is the drag coefficient. Note that the jet responds to this force through deformation of its surface and/or jet displacement. c_D may be estimated from the characteristics of the vortex wake downstream of the jet in a manner described by Goldstein;[17] however, here we assume that for $\epsilon \ll 1$, over the region of interest, it remains sensibly constant, the value of which is to be determined from experiment. From (2), $d(z)$ is given by

$$d(z)/a = 2[1 + \xi^2 + O(\xi^4)]. \tag{4}$$

We consider the control volume V between the orifice and a section CD enclosed by the surface S shown in Fig. 2(b). From the integral momentum theorem (see Batchelor[18]) we have for steady flow in the jet,

$$\int_s \rho_j \mathbf{u}(\mathbf{u}_j \cdot \mathbf{n}) dA = -\int_s p\mathbf{n}\, dA, \tag{5}$$

where the subscript j refers to quantities associated with the jet and the normal $\mathbf{n}$ points outwards from the control volume. Then assuming no mass transfer in the near jet region, $\mathbf{u}\cdot\mathbf{n} = 0$ everywhere on S except at the cross-sectional surfaces AB and CD where $\mathbf{u}\cdot\mathbf{n} = U_{\text{jet}}$ to $O(\xi^4)$ in view of continuity of mass. Thus the contribution to the integral on the left-hand side of (5) will come from AB and CD. At AB $\mathbf{u} = (0, 0, U_{\text{jet}})$ while at CD, if the angle between the normal $\mathbf{n}$ and OZ is μ, we can write to $O(\xi^4)$, $\mathbf{u} = (U_{\text{jet}} \sin\mu, O, U_{\text{jet}} \cos\mu)$. In view of the continuity of pressure across the jet surface, we can relate the horizontal (x) component of force on the right-hand side of (5) to the flow drag associated with the pressure differences between the windward and the leeward sides of the jet generated by the presence of wake vortices due to separation off the rigid pipe surface. Thus, using (3), we have

$$\rho_j U_{\text{jet}}^2 A \sin\mu = \frac{1}{2}\,\rho_\infty U_\infty^2 \int_0^z c_D d(z_1) dz_1\,, \tag{6}$$

where $A = \pi a^2[1 + O(\xi^4)]$ is the cross-sectional area and ρ_∞ refers to the density of the ambient fluid. On substituting for $d(z)$ from (4), we have

$$\sin\mu = \frac{\rho_\infty}{\pi\rho_j}\,\epsilon^2 c_D\left(\frac{z}{a}\right)\left\{1 + \frac{\xi^2}{3} + O(\xi^4)\right\}. \tag{7}$$

Then, using $dx_c/dz = \tan\mu$, we obtain that for small μ, the x coordinate ($x = -x_c$) of the location of the jet center is given by

$$\frac{x_c}{a} = \beta\{\xi^2 + O(\xi^4)\}, \tag{8}$$

where $\beta (= \rho_\infty C_D/2\pi\rho_j)$ is a constant; its value would need to be determined from experiment. In view of this displacement, (2) may be replaced by

$$\frac{r_b(\theta,\xi)}{a} = 1 - \xi^2(\beta\cos\theta + \cos 2\theta) + O(\xi^4). \tag{9}$$

It may be noted that this has no effect on the cross-sectional shape predicted by (2). However, it predicts that the initial trajectory of the centerline is such that its height $z_c \propto \epsilon^{-1} x_c^{1/2}$. Coelho and Hunt[15] obtained the relation $z_c \propto \epsilon^{-1/2} x_c^{1/2}$ using their turbulence entrainment model; they report, however, that in most experiments the relation $z_c \propto \epsilon^{-b} x_c^e$ is obtained where $0.47 < b < 1$ and $0.33 < e < 0.39$. On comparing the displacement given by (8) with present experimental results, we find that $\beta = 1.4$ gives good agreement. Note, however, that in general, β is likely to be dependent upon Reynolds number and existence of shear in the free stream. The analysis suggests that jet tilting is initiated by the presence of vortical structures, in the near wake of the jet, which arise from shedding off the surface of the rigid pipe. The side and front views corresponding to Fig. 3, after taking account of the jet displacement are given in Fig. 4. The model fails to predict the deflection in the downstream direction quite close to the orifice observed in the current experiments (see Fig. 8); this may be due to a strong interaction between the free stream and the edge of the orifice, not accounted by the model.

The vertical component of (5) becomes

$$\rho_j U_{\text{jet}}^2 A(\cos\mu - 1) = -\int_s p(\mathbf{n}\cdot\mathbf{k}) dA \tag{10}$$

implying, in view of (7) an $O(\rho_j U_{\text{jet}}^2 A \epsilon^2 \xi^2)$ net force on the control volume in the negative z direction; this force, which does not concern us here, is identified with the Kutta-lift force due to the action of the cross-flow on the azimuthal vorticity on the jet boundary (together with the buoyancy force on the control volume, if appropriate). The Kutta-lift force has a net zero value if the jet is straight since its value on the windward side is equal and opposite to that on the leeward side; however, an imbalance in these forces occurs if the jet is tilted since the region of the control volume on the windward side now exceeds that on the leeward side, resulting in a net vertically downward force.

III. EXPERIMENTAL APPARATUS

The experiments were conducted in a recirculating water tunnel. The tunnel is constructed from plexiglass and has an observation section 160 cm long, 22 cm high and 20 cm wide. The top surface over the length of the observation section is free. The flow is driven by a small pump.

The jet nozzle, which was formed from a cylindrical steel pipe of internal radius $a=0.1$ cm, was aligned vertically, perpendicular to the cross-flow. The pipe was rigidly mounted. The end of the jet nozzle was located 2 cm (i.e., $20a$) above the floor of the tunnel, exterior to the bottom boundary layer. The bottom boundary layer thickness, defined by $0.99U_\infty$, were approximately 1 cm, where U_∞ is the mean velocity of the cross-flow far from the boundary layer so that the jet discharged into a uniform cross-flow. The jet was supplied from a reservoir, and driven by a second independent pump. The flow through the jet was controlled by a valve which was located upstream of the jet nozzle. The jet discharge was calibrated before and after each experiment, and discharge rates were repeatable to within 5%. To avoid undesired buoyancy effects, the density and temperature of the water in the tunnel and the jet reservoir were carefully monitored. Densities were measured by a refractometer, and temperature by a thermometer. Differences in density and temperature between the water in the tunnel and the water in the jet reservoir were less than 0.02% and 0.1 °C.

To visualize the flow field, a small amount of methylene blue dye was added to the jet reservoir water: this did not change the density measurably. A motor driven camera with 400 ASA film, operated at a shutter speed of 1/125 s was used to photograph the flow. Grids of 5 and 20 cm spacings were marked on the floor of the tunnel and on one sidewall to facilitate scaling from photographs. A mirror was positioned at 45° to the water surface over the observation section: this enabled simultaneous views of the y, z and x, z planes (i.e., plan and elevation views). Measurements of the geometry of the near-field were determined from projection of the negatives and from enlargements of photographs. Errors in measuring position and dimensions of flow features were minimized by using grid markings in the vicinity of the flow feature that was being measured—errors were typically less than 5%.

Two component (u,w) turbulent velocity measurements are obtained with a quartz-coated cylindrical x-film probe (Type TSI 1241-20W) operated at 2% overheat by a AN1003 anemometer unit. To correct for the small length (0.20 cm) to diameter (0.015 cm) ratio of the x-film probes yaw corrections with $k=0.35$ are applied (see Huq and Britter[19] for further details). Mean velocities were also measured by tracking the vertical traces of Potassium Permanganate (KM_NO_4) crystals, less than 0.05 cm in diameter, which were dropped in the observation section. Mean velocities were found to be homogeneous except for the boundary layers at the sidewalls and bottom which grew to 1 cm. Mean velocities were repeatable to within 5%. Efforts to measure the pipe exit velocity profile by the hot-film probe were unsuccessful as the dimensions of the hot-film probes and support were similar to the pipe diameter so that there was disturbance to the flow field. However, the pipe exit velocity profile is likely to be similar to the profiles measured (by hot wires) by Kamotani and Greber[3] and Moussa *et al.*[6] Kamotani and Greber found a top-hat profile at $z/2a=0$ (see their Fig. 6): further from the exit at $z/2a\approx 1$ both Kamotani and Greber and Moussa *et al.* also found approximate top-hat profiles [see their Figs. 6 and 15(a) respectively]. For all experiments the water depth of the crossflow was 18 cm. Also for all experiments the jet discharge was kept constant at $Q=0.33$ cm^3/s, so that for the 0.1 cm radius jet nozzle, $U_{\text{JET}}=10.5$ cm/s and the value of the Reynolds number $R=2aU_{\text{JET}}/\nu$ was 210. The mean velocity U_∞ of the cross-flow was varied between 1.1–3.9 cm/s. Thus values of the ratio ϵ varied between 0.10–0.37.

An additional series of experiments were conducted to map the velocity and scalar concentration fields emanating from the jet discharge. For these experiments for which the water depth was 30 cm, the pipe was also rigidly mounted, the diameter of the jet was 0.36 cm, $U_\infty=8.3$ cm/s and the velocity ratios U_∞/U_{JET} were 0.32 and 0.13 with Reynolds numbers $R=930$ and 2300, respectively. The marked scalar was effected by adding brine to the jet discharge, and dissolving household sugar to the fluid of the recirculating water tunnel till the densities matched. The value of the Schmidt number $S_c=\nu/\kappa$, the ratio of the scalar to momentum diffusivity, was 700. This enabled an aspirating conductivity to map the scalar concentration field. An aspirating conductivity probe, which was capable of precisely traversing the flow field in x, y, and z directions, was operated in an AC bridge at 1 KHz. The spatial resolution of the probe was estimated to be 0.04 cm; and the frequency response was 70 Hz. Constant salinity baths were used to calibrate the probe. Signals were recorded on FM tape, and the data were subsequently digitized at 50 Hz and stored on flexible discs. Statistical analyses was undertaken using standard software.

A referee has validly suggested that tip effects associated with possible vibrations of the pipe or with the 3-D flow past a free-ended pipe can induce the jet to bifurcate. The issue of vibration of the jet exit as well as the presence of random acoustic disturbances in the environment is important. Parekh and Reynolds[12] show how acoustic forcing of a round jet, in the absence of a cross-flow, can induce jet instability; they show that at a fairly high Reynolds number of 10^5, a circular jet can exhibit pronounced 3-D behavior even in the absence of acoustic forcing. In our experiments, the jet Reynolds numbers are much smaller than in the experiments of Parekh and Reynolds. Furthermore, the pipe was rigidly

mounted and care was taken to ensure absence of any external disturbances to the flow. The location at which bifurcation occurred was repeatable and did not change when either of the two pipes used in the experiments was employed, suggesting that the observed bifurcation cannot be attributed to random acoustic noise. Regarding the issue of flow past a free-ended pipe, we believe that for the small values of ϵ at which bifurcation was observed, the jet has sufficient momentum in the near field to counter the end effects of the type which are observed in flow past free-ended cylinders. No such adverse tip effects were apparent in the experiment.

IV. RESULTS

Experiments were undertaken for values of the velocity ratio $\epsilon=0.37$, 0.32, 0.29, 0.25, 0.20, 0.13, and 0.10. However, to establish trend, the results of flow visualization, in particular plan (x,y) and elevation (x,z) views, are shown in Fig. 5 only for three different values of the velocity ratio ϵ. For $\epsilon=0.37$ the jet does not bifurcate, and the flow field comprises of tangled vortical structures which resemble those discussed by Perry and Lim.[20] Observations showed that these structures possessed vorticity and were not advecting flow patterns devoid of vorticity: the structures persist for distances beyond 400 $x/2a$. The structures, which originate close to the source, grow with distance from the source. For $\epsilon=0.37$ at $x/2a=50$ both the maximum height and width were $13a$. By $x/2a=300$ both the maximum height and width had grown to $20a$. The average spacing between the structures was $14a$. Values of the Strouhal number $S_T=2af/U_\infty$, which is the frequency at which the vortical structures are swept past a point, were determined using values of f calculated by dividing the average spacing between the structures by U_∞. Values of S_T for $\epsilon=0.37$ and 0.29 were 0.07 and 0.08, respectively. It is known that $S_T\sim0.1$ for shedding past a circular cylinder at the range of low Reynolds numbers of the present experiments (Roshko[21]). Thus the approximate accord of the present values of $S_T=0.07$ and 0.08 with $S_T\sim0.1$ for flow past a circular cylinder suggests that shedding from the pipe plays a dominant role in the dynamics. A similar interpretation of Strouhal numbers for flow emanating past an ''unskirted'' pipe in a crossflow was given by Moussa *et al.*[6] Moussa *et al.* undertook hot-wire measurements (but without visualizations) mostly for $\epsilon=0.29$ for $x/2a\leqslant4$. They did not observe bifurcation; however, on the dependence of the Strouhal number on the velocity ratio, ϵ, they noted ''there seem to be two regimes, the change from one to the other occurring near $U_{\mathrm{JET}}/U_\infty=5.5$'' (i.e., $\epsilon=0.18$).

Figure 5 shows clearly that the jet bifurcates for $\epsilon=0.25$ and 0.20. The principal feature of the flow field is the presence of two distinct counterrotating arms (in the x-y plane). Bifurcation of the jet occurs for $\epsilon=0.10$, 0.20, and 0.25 but not for $\epsilon=0.29$ and 0.37. The data thus indicates a critical value of ϵ, $\epsilon_{\mathrm{CRIT}}\approx0.25$, as the criterion for the bifurcation of a circular jet in a cross-flow.

Figure 6 shows visualizations which are perspective views of the source region for $\epsilon=0.37$, 0.25, and 0.20. It is evident that the structure of the flow field of the jet differs for $\epsilon=0.37$ in comparison to $\epsilon=0.25$ and 0.20 from small values of $x/2a$. For $\epsilon=0.37$ the flow field organizes into tangled vortical structures by $x/2a=20$. In contrast, for $\epsilon=0.25$ and 0.20 the visualizations show that the jet bifurcates close to the jet exit (by $x/2a<10$). The two arms of the bifurcated jet are linked or bridged by structures which are similar in form to the shear layer ring vortices observed by Fric and Roshko.[9] For $\epsilon=0.25$ the linkages or bridges between the

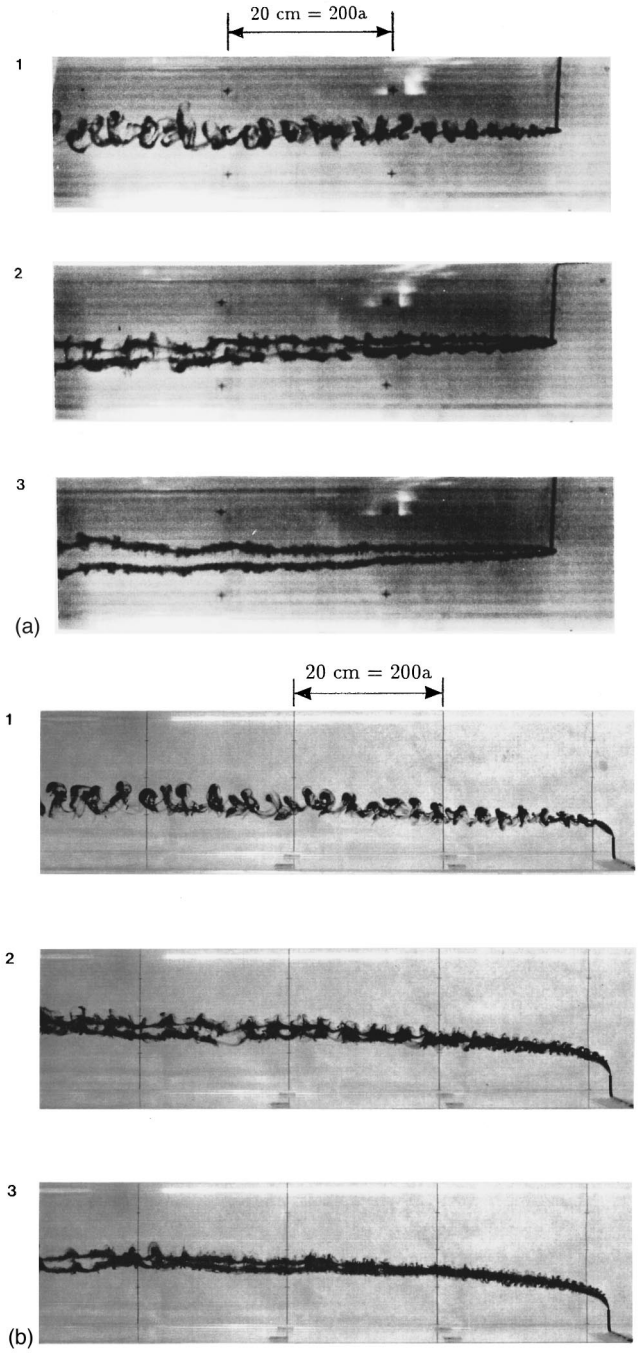

FIG. 5. (a) Visualizations showing plan views (x-y plane) for three different values of the velocity ratio ϵ (1) $\epsilon=0.37$; (2) $\epsilon=0.25$; (3) $\epsilon=0.20$. Crosses indicate a grid spacing of 20 cm$=200a$ in the x direction, and 10 cm$=100a$ in the y direction. (b) Visualizations showing elevation views (x-z plane) for three different values of the velocity ratio ϵ, (1) $\epsilon=0.37$; (2) $\epsilon=0.25$; (3) $\epsilon=0.20$. Vertical lines indicate a grid spacing in the x direction of 20 cm $=200a$.

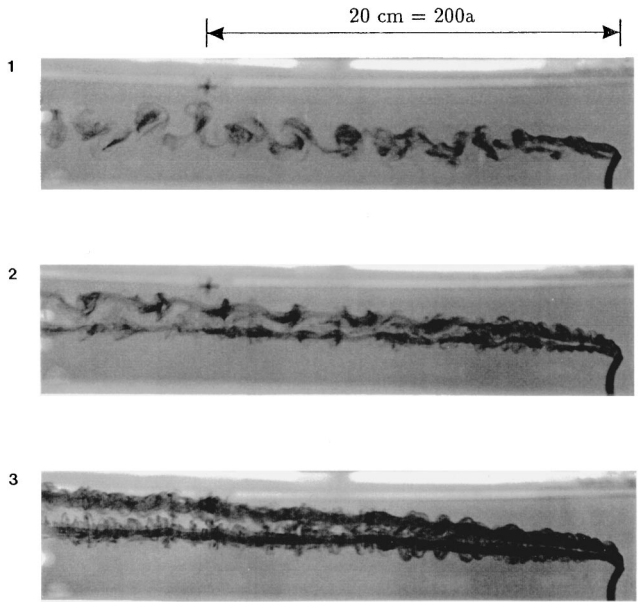

FIG. 6. Visualizations showing perspective view of jet exit region for three different values of the velocity ratio ϵ, (1) ϵ=0.37; (2) ϵ=0.25; (3) ϵ=0.20.

two arms of the jet are visible upto $x/2a\sim25$, whereas for ϵ=0.20 the bridges persist upto $x/2a\sim40$.

For larger distances from the source ($x/2a>50$) two distinct arms exist for both ϵ=0.25 and 0.20. It is seen in Fig. 6 that for ϵ=0.25 and 0.20 that the vorticity in each arm generates small scale structures that are wrapped around the core of each arm. For ϵ=0.25 the trajectories of the arms of the jet are more convoluted than for the arms of the jet for ϵ=0.20. Examination of Fig. 5(a) shows that convolutions, which are visible on both x-y and x-z planes, occurs even at large distances ($x/2a\sim300$). For example, at $x/2a\sim225$ and $x/2a\sim260$ the convolutions are large: indeed so large that renewed bridging between the two arms can be seen. In contrast, for ϵ=0.20 [Fig. 5(a)] though there are convolutions at large values of x/a (e.g., at $x/2a\sim225$), the two arms of the jet are not bridged beyond $x/2a\sim40$.

The trajectory of the jets in the x-z plane were determined from best fit lines through the center of the structures. The results are shown on Fig. 7. Figure 7(a) shows that there is region of steep rise up to $x/2a\sim100$ in which $z\sim x^{1/2}$ in accord with Eq. (9). The trajectory for $x/2a>100$ is less steep with $z\sim x^{0.3}$ approximately. Figure 7(a) also shows a dependence of the trajectory on ϵ. This is shown explicitly on Fig. 7(b) for values of z at x/a=3 for various values of ϵ. The limited data are consistent with a $z\sim\epsilon^{-1}$ dependence in accord with Eq. (9).

The near-field geometry of the jet in the x-z plane is shown in Fig. 8. For both ϵ=0.1 and 0.25 the jet is bent by the cross-flow. The rate of bending is greater for ϵ=0.25 than for ϵ=0.1 because, as $\epsilon=U_\infty/U_{\mathrm{JET}}$, larger values of ϵ correspond to a stronger cross-flow. Also shown on Fig. 8 are the predictions of 2-D and 3-D analyses. For both ϵ=0.1 and 0.25 there is good agreement with the analyses though the analyses overpredicts the width of the jet close to the jet exit. The observed contraction or narrowing of the flow near the

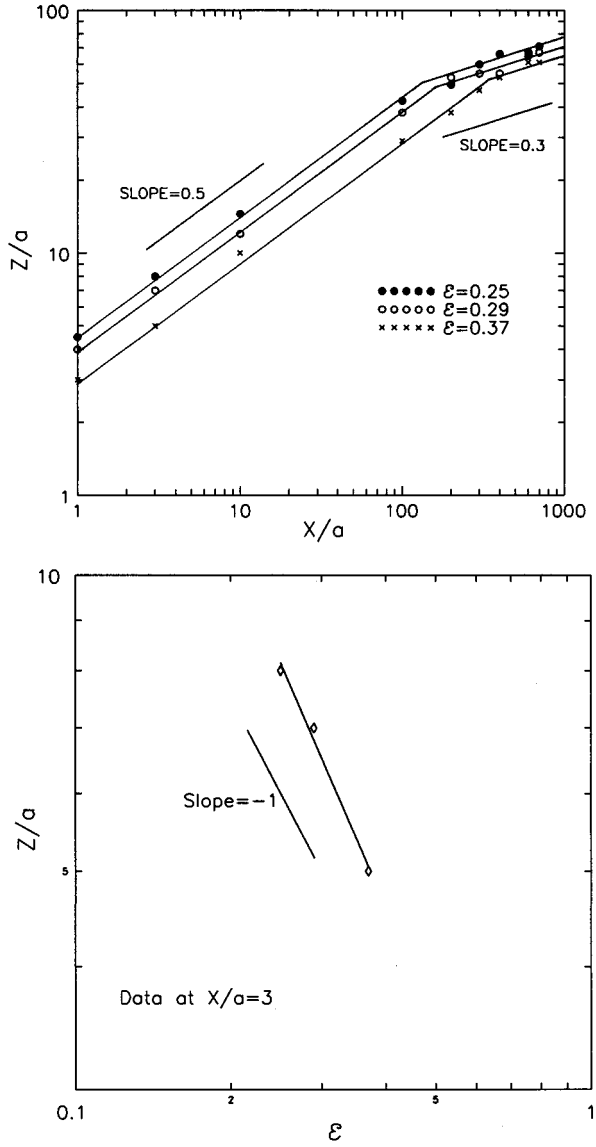

FIG. 7. (a) Trajectory of centerline of jet showing $z\sim x^{1/2}$ and $z\sim x^{0.3}$ power law growths. Only data for $\epsilon\geqslant$0.25 shown as bifurcation occurs for $\epsilon<$0.25. (b) Dependence of trajectory on the velocity ratio ϵ. Data taken at z/a=3 from (a). Note that both ordinate and abscissa are log scales. Also shown is a−1 power law slope. Note only data for $\epsilon\geqslant$0.25 shown as bifurcation occurs for $\epsilon<$0.25.

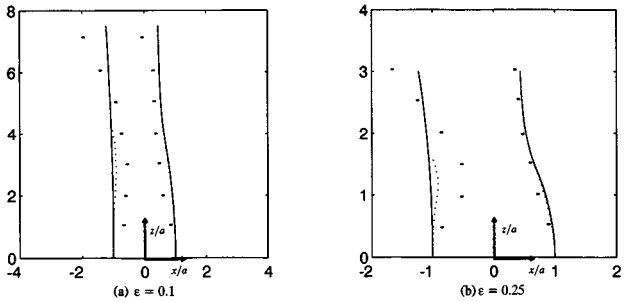

FIG. 8. Near-field elevation geometry of jet (x-z plane). Predictions of 3-D calculations [——; Eq. (9) with β=1.4], two-dimensional calculation [⋯ ; Eq. (1)] but with inclusion of downstream drift as in Eq. (9), and corresponding experimental data points (–) are shown.

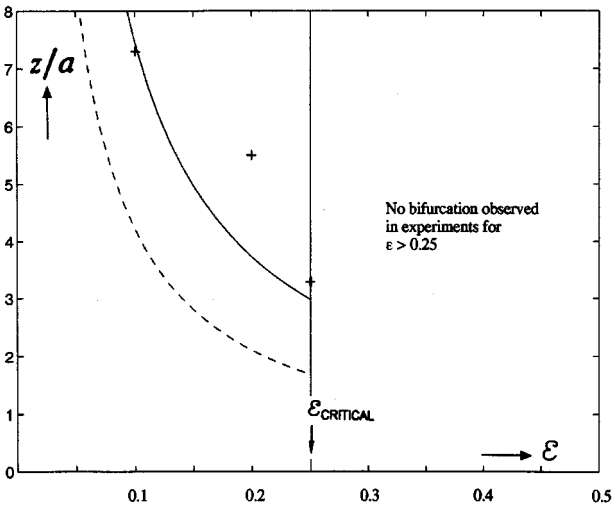

FIG. 9. Value of z/a at which jet bifurcates for a given value of ϵ according to the 2-D (----) and three-dimensional (——) models. "+" refers to the values observed in the experiment. Only data for $\epsilon \leqslant 0.25$ is shown as no bifurcation observed for $\epsilon > 0.25$.

jet exit is not predicted by the potential flow 3-D model and is underpredicted by the 2-D model.

The vertical location at which the jet bifurcated was determined from enlargements of visualizations. The experimental data for the vertical location of the point of bifurcation are shown in Fig. 9. The data shows that for small values of ϵ, that is for relatively weaker cross-flows, the jet penetrated for greater vertical distances before bifurcation. The agreement of the experimental data with 3-D bifurcation criteria discussed in Sec. II is again good. At the critical value of ϵ of 0.25, the value of the aspect ratio α of the the elliptic cross section of the jet was found to be 3.2. This is in accord with the suggestion[16] of a critical ellipticity of $\alpha = 3.5$.

The angle of separation between the arms of the bifurcated jet is constant at large distances (i.e., $x/2a > 50$) except

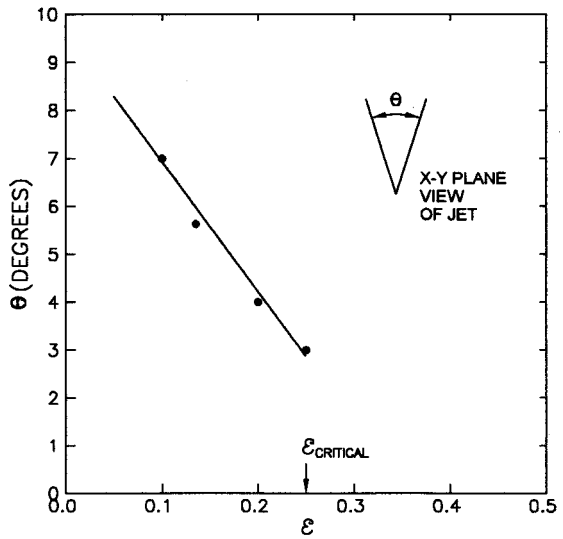

FIG. 10. Dependence of horizontal spreading angle θ between arms of bifurcated jet and velocity ratio ϵ. Only data for $\epsilon \leqslant 0.25$ is shown as no bifurcation observed for $\epsilon > 0.25$.

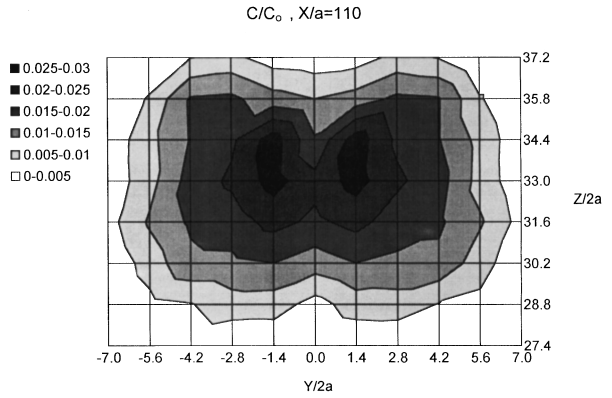

FIG. 11. Nondimensional mean concentration contours $\bar{c}/\bar{c}_0$ for $\epsilon = 0.32$ at $x/a = 110$. $\bar{c}_0$ is the scalar concentration at the jet exit. Note that data were obtained for positive values of $y/2a$ and reflected to generate an image for negative values of $y/2a$.

for the previously discussed occurrence of interactions between the arms which results in isolated convolutions and bridges between the arms of the jet. Figure 10 shows the angle of separation, θ, to depend on ϵ, with the value of the spreading angle greater for smaller values of ϵ (e.g., for $\epsilon = 0.1$, $\theta = 7°$; $\epsilon = 0.25$, $\theta = 3°$).

Figures 11 and 12 are maps in the y-z plane of mean concentrations for nonbifurcated and bifurcated jets ($\epsilon = 0.32$ and 0.13, respectively). The maps were determined from measurements taken at the intersection points of the grids (i.e., effective mesh spacing was $2.8a$) of Fig. 11 and 12. Data were collected for positive values of $y/2a$ and reflected to generate an image for negative values of $y/2a$. Figure 11 shows concentration contours for $\epsilon = 0.32$. There is a core of approximate diameter of $2a$ of relatively high concentration located off the center axis ($y/2a = 0$) of the jet. The maximum value of the concentration in the core is $\bar{c}/\bar{c}_0 = 0.03$ which implies a dilution of $(\bar{c}_0/\bar{c})$ of 33. The concentration contours are approximately equally spaced; the scalar distribution suggests that the structure comprises of two vortices: similar distributions were observed by Kamotani and Greber.[3] The dimensions of the inferred vortices is approximately $14a$ in height and $12a$ width, thus the aspect ratio of

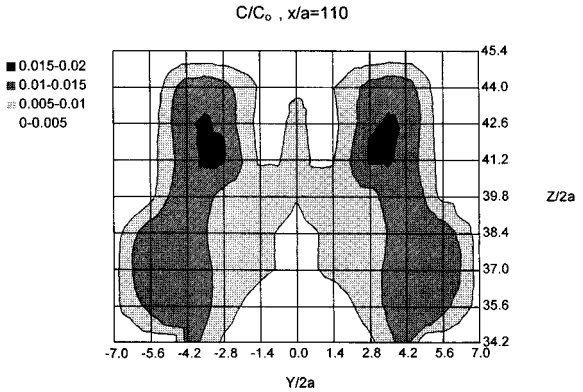

FIG. 12. Nondimensional mean concentration contours $\bar{c}_0$ for $\epsilon = 0.13$ at $x/a = 110$. Note that data were obtained for positive values of $y/2a$ and reflected to generate an image for negative values of $y/2a$.

the overall jet (i.e., twice the vortex width to the vortex height) is about 1.7 at $x/a=110$.

Figure 12 shows the concentration contours for the jet with $\epsilon=0.13$. The scalar distribution also suggests a structure comprising two vortices, each with a core of relatively high concentration located off the center of the jet axis. Examination of concentration contours for $\epsilon=0.32$ shows that the relatively high concentration cores are separated by a nondimensional distance $y/2a\approx2.8$. In comparison the contours for $\epsilon=0.13$ shows that the high concentration cores are more separated as the nondimensional distance between the cores is $y/2a\approx7$, and bifurcated as each branch (or inferred vortex) is almost completely enveloped by zero concentration fluid from outside of the jet. The nonuniform spacing of the contours for $\epsilon=0.13$ suggests that the structure of the inferred vortices are not circular, but rather are very approximately elliptical, with a value of the aspect ratio of the major to minor axis for the $\bar{c}/\bar{c}_0=0.01$ contour being about 3.5. Also the orientation of the contours suggest that the major axis is inclined at 15° to the vertical. The maximum value of the concentration within the core is $\bar{c}/\bar{c}_0=0.02$ which implies a dilution of 50. This suggests that dilutions for bifurcated jets are greater.

Frequency spectra determined from concentration time series are shown in Fig. 13 for $\epsilon=0.32$. The three spectra are taken at $y/2a=2.8$ for $z/2a=37.2$, 33.0, 28.8 that is at the top, center and bottom of the jet (see Fig. 11). This is done to check if the characteristic frequencies of the jet structure at the top, center, and bottom differ. Figure 13 shows that the forms of the spectra are similar: uncertainty grows at low frequencies due to the finite length of the time series, and spectral densities decrease for frequencies larger than 2 Hz upto the Nyquist frequency of 25 Hz. There are no frequencies with distinct spectral density peaks. This is in contrast to the periodicity which is evident in the visualizations of Figs. 5(a) and 5(b). For the flow fields of Figs. 5(a) and 5(b), a periodicity of 1.3 Hz is obtained by dividing the average spacing between the structures by U_∞ for both $\epsilon=0.37$ and 0.29, respectively. The contrast between a peak at the Strouhal frequency in the spatial domain and a flat frequency spectra in the time domain indicates phase jitter (i.e., random fluctuations) of the advecting structures. In frequency spectra the effect of phase jitter of advecting structures is to flatten the spectra so as to weaken periodicity which exists in the spatial domain. Figure 13 suggests that the phase jitter of the structures which are visible in Figs. 5(a) and 5(b) occurs at frequencies of the same order as that corresponding to the passage of the structures (i.e., at the Strouhal frequency). The similar form of the spectra in Fig. 13 at the top, center, and bottom of the jet suggests that jitter of the jet occurs throughout the vertical extent of the jet, that is that the jet structure is effectively rigid.

This is also supported by measurements of the velocity field of Figs. 14 and 15. Figure 14 shows values of the root-mean-square velocities u' and w' nondimensionalized by the free-stream velocity U_∞. Maximum values of u' and w' occur in the center of the jet, with decay above and below. There is a local increase in the value of u' and w' at the bottom edge of the jet at $z/2a=21$ which may be attributed

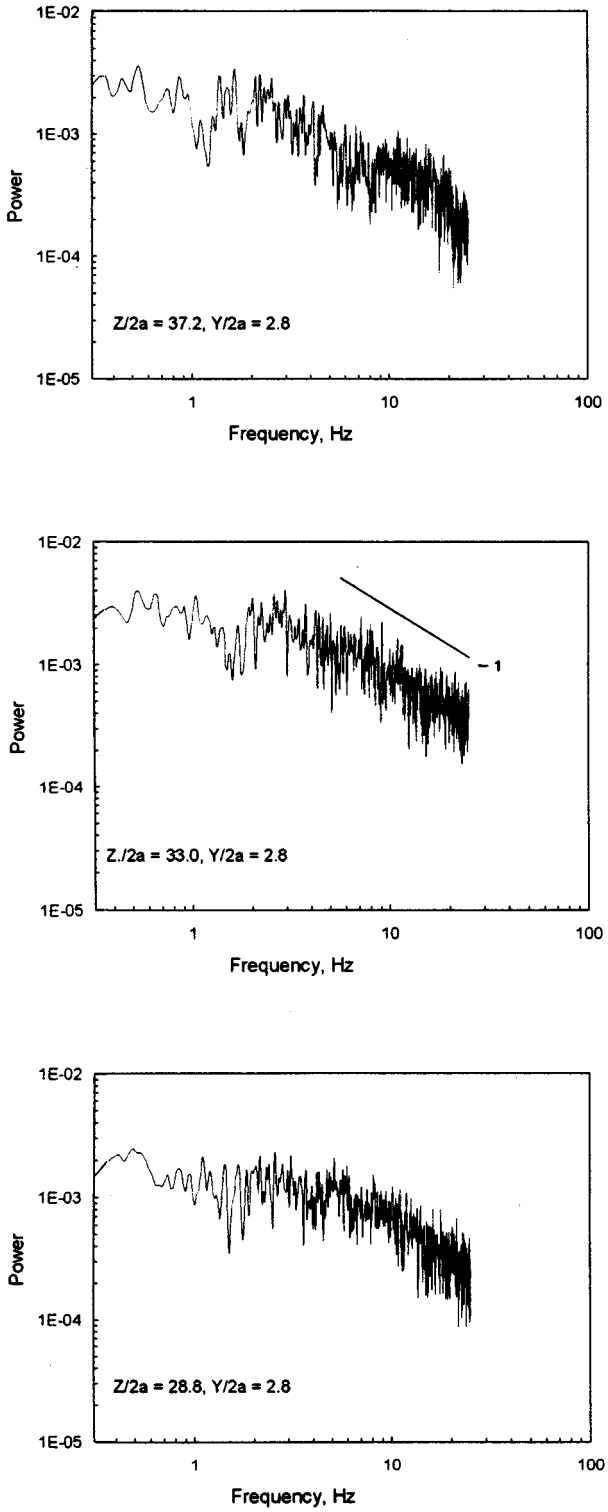

FIG. 13. Frequency spectra for concentration for $\epsilon=0.32$ at $x/a=110$. Spectra are for points located along a transect $y/2a=2.8$ at $z/2a=37.2$, 33.0, 28.8 corresponding to the top, middle, and bottom of the jet structure (see Fig. 11). Nyquist frequency is 25 Hz.

to vortex shedding off the pipe of the jet nozzle (Moussa *et al.*[6]). Figure 15 shows the frequency spectra for the w velocity component near the top, center and bottom of the jet. As for the scalar spectra, the bulk of the spectral energy for velocity fluctuations resides in the lower frequencies without a distinct spectral peak at the Strouhal frequency

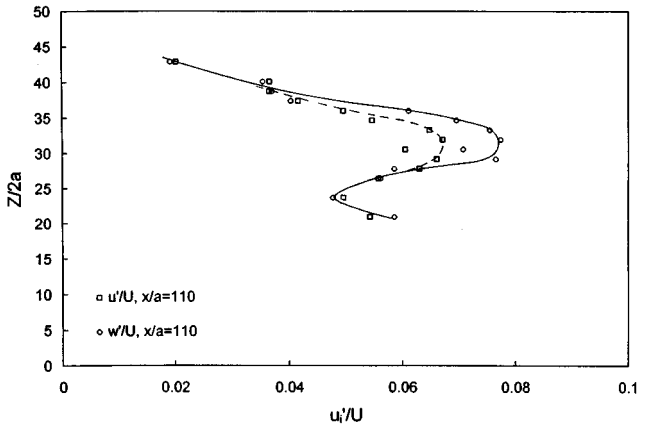

FIG. 14. Distribution of nondimensional velocity variances u' and w'. Data were taken along a vertical transect at $x/a=110$, $y/2a=0$. The value of the velocity ratio $\epsilon=0.32$. Note that variances u_i' were nondimensionalized by the free-stream velocity of 8.3 cm/s.

($\approx$1.3 Hz). This suggests that the vortices shed from the pipe are also subject to phase jitter.[10] Note that these measurements were taken at $x/a=110$. In comparison previous measurements[6,9,10] were taken at $x/a<15$. The relatively large dimensions of hot-film probes, in comparison to hot wires, used for these water tunnel experiments preclude measurements for small values of x/a. Comparison of scalar and velocity spectra shows that velocity spectra falls more steeply than scalar spectra (approximately f^{-1} as opposed to f^{-2}) which is to be expected for these high Schmidt number flows.

V. CONCLUSIONS

In this paper, an experimental study of a circular incompressible jet in a cross-flow is described and the results are compared with existing potential flow models. The objective of the study was to investigate the conditions under which bifurcation of the jet occurred.

The jet exited in a region of uniform cross-flow, from a pipe projecting above the floor of the tunnel, above the bottom boundary layer near the floor of the tunnel. For this present configuration the jet–cross-flow interaction results in a bent-over jet which is observed to bifurcate close to the jet exit for a range of values of ϵ. A critical value of the parameter $\epsilon=U_\infty/U_{\mathrm{JET}}$, the ratio of the mean velocity U_∞ of the crossflow to the mean jet discharge velocity U_{JET}, defines when bifurcation occurs: bifurcation occurs at a finite distance from the jet exit if $\epsilon\leqslant 0.25$. The structure of the flow field for jets with $\epsilon>0.25$ comprises tangled vortical structures which survive for very long distances x from the jet exit, beyond $x/2a>400$ where a is the radius of the jet.

The jet cross section becomes elliptical in response to variation of pressure around the jet. The aspect ratio of the ellipse increases with distance away from the jet exit. If U_∞ is small enough (i.e., $\epsilon<0.25$), then the aspect ratio increases until it is $\sim$3.5 when bifurcation occurs. This is in agreement with analysis based on consideration of a 3-D potential flow model and characteristics of bifurcating elliptical jets.

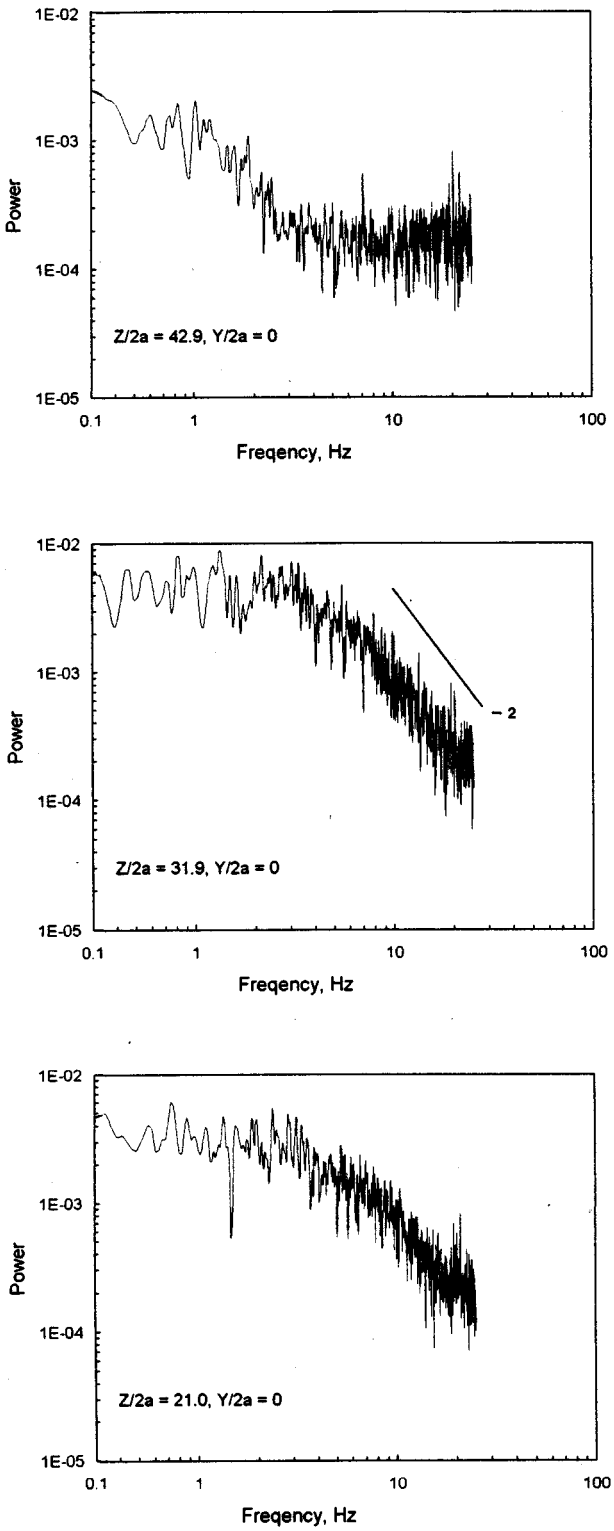

FIG. 15. Frequency spectra for w velocity fluctuations for $\epsilon=0.32$ at $x/a=110$. Spectra are points located along a transect $y/2a=0$ at $z/2a=42.9$, 31.9, 21.0 corresponding to the top, middle, and bottom of the jet structure. Note the absence of peaks near the vicinity of the Strouhal frequency of 1.3 Hz.

The location of the point of bifurcation is further from the jet exit for smaller values of ϵ. The structure of the flow field after bifurcation consists of two counter-rotating arms whose vorticity fields generates small-scale structures

wrapped around the core of each arm. The angle of separation between the arms of the bifurcated jet is found to vary inversely with ϵ for $\epsilon \leqslant 0.25$. If U_∞ is moderately large ($0.37 < \epsilon < 0.25$), the jet instability occurs before the critical aspect ratio is attained, so that the flow appears to behave like a forced jet with forcing frequencies of the order of the shedding frequency. This is presumably related to flow separation and Karman vortex shedding in the wake of the pipe, and results in the appearance of coherent distorted ring-like vortical structures. The trajectory of the jet rise is found to vary as $z \sim x^{1/2}$ and $z \sim \epsilon^{-1}$ for small distances in agreement with 3-D analysis for both bifurcated and nonbifurcated jets. For both bifurcated and nonbifurcated jets, the vortical structures which ensue the jet instability are found to persist for very long distances, beyond $x/2a > 400$.

Mapping of the mean scalar concentration shows the mixture of a core of relatively high concentration within the jet structure for both bifurcated and nonbifurcated jets. For nonbifurcated jets the structure of the jet comprises of two circular vortices. In contrast, for bifurcated jets the structure comprises approximately elliptical vortices which are inclined at 15° to the vertical. Dilutions for bifurcated jets are greater. Measurements of the turbulent velocity field showed local increases in velocity variances in the vicinity of the jet exit due to vortex shedding off the pipe: however, time domain frequency spectra of the velocity (and also scalar) signal showed no peaks near Strouhal frequencies at $x/a = 110$. This is consistent with phase jitter or random fluctuations from periodicity of the advecting vortical structures.

ACKNOWLEDGMENTS

This research was partially funded by grants from the Electric Power Partners and the University of Delaware Research Foundation.

[1] J. F. Keffer and W. D. Baines, "The round turbulent jet in a cross-wind," J. Fluid Mech. **15**, 481 (1963).
[2] H. M. McMahon, D. D. Hester, and D. D. Palfrey, "Vortex shedding from a turbulent jet in a cross-wind," J. Fluid Mech. **48**, 73 (1971).
[3] Y. Kamotani and I. Greber, "Experiments on a turbulent jet in a cross flow," AIAA J. **10**, 1425 (1972).
[4] R. Fearn and R. P. Weston, "Vorticity associated with a jet in a cross flow," AIAA J. **12**, 1666 (1974).
[5] P. Chassaing, J. George, A. Claria, and F. Sananes, "Physical characteristics of subsonic jets in a cross-stream," J. Fluid Mech. **62**, 41 (1974).
[6] Z. M. Moussa, J. W. Trischka, and S. Eskinazi, "The near field in the mixing of a round jet with a cross-stream," J. Fluid Mech. **80**, 49 (1977).
[7] D. Crabb, D. F. G. Durao, and J. H. Whitelaw, "A round jet normal to a crossflow," J. Fluids Eng. **103**, 142 (1981).
[8] J. Andreopoulos and W. Rodi, "Experimental investigation of jets in a crossflow," J. Fluid Mech. **138**, 93 (1984).
[9] T. F. Fric and A. Roshko, "Vortical structure in the wake of a transverse jet," J. Fluid Mech. **279**, 1 (1994).
[10] O. S. Eiff, J. G. Kawall, and J. F. Keffer, "Lock-in of vortices in the wake of an elevated round turbulent jet in a crossflow," Exp. Fluids **19**, 203 (1995).
[11] R. S. Scorer, *Environmental Aerodynamics* (Ellis Horwood, Chichester, 1978), p. 365.
[12] D. E. Parekh and W. C. Reynolds, "Forced instability modes in a round jet at high Reynolds numbers," Phys. Fluids A **1**, 1447 (1989).
[13] H. Chang-Lu, "Aufrallung eines zylindrischen strahles durch queswind," Doctoral thesis, University of Goettingen, 1942.
[14] D. J. Needham, N. Riley, and J. H. B. Smith, "A jet in crossflow," J. Fluid Mech. **188**, 159 (1988).
[15] S. L. V. Coelho and J. C. R. Hunt, "The dynamics of the near field of strong jets in crossflows," J. Fluid Mech. **200**, 95 (1989).
[16] F. Hussain and H. S. Husain, "Characteristics of unexcited and excited jets," J. Fluid Mech. **208**, 257 (1989).
[17] S. Goldstein, *Modern Developments in Fluid Dynamics* (Dover, New York, 1965), Vol. 2, Chap. XIII.
[18] G. K. Batchelor, *An Introduction to Fluid Dynamics* (Cambridge University Press, Cambridge, 1967), Sec. 6.3, p. 387.
[19] P. Huq and R. E. Britter, "Mixing of a two-layer scalar profile due to grid-generated turbulence," J. Fluid Mech. **285**, 17 (1995).
[20] A. E. Perry and T. T. Lim, "Coherent structures of coflowing jets and wakes," J. Fluid Mech. **88**, 451 (1978).
[21] A. Roshko, "On the development of turbulent wakes from vortex streets," NACA TN No. 2913, 1953.